Magnetic particle characterization in the Seine river system: Implications for the determination of natural versus anthropogenic input

Christine Franke

Laboratoire des Sciences du Climat et de l'Environnement, IPSL, CEA, UVSQ, CNRS, Campus du CNRS, Bâtiment 12, Avenue de la Terrasse, F-91198 Gif-sur-Yvette CEDEX, France

Now at Centre des Géosciences, Ecole des Mines de Paris, 35 rue Saint-Honoré, F-77305 Fontainebleau CEDEX, France (christine.franke@mines-paristech.fr)

Catherine Kissel, Eric Robin, and Philippe Bonté

Laboratoire des Sciences du Climat et de l'Environnement, IPSL, CEA, UVSQ, CNRS, Campus du CNRS, Bâtiment 12, Avenue de la Terrasse, F-91198 Gif-sur-Yvette CEDEX, France

France Lagroix

Equipe de Paléomagnétisme, Institut de Physique du Globe de Paris, Université Paris-Diderot, CNRS, 4 place Jussieu, F-75252 Paris CEDEX 05, France

[1] This study presents an innovative application of well-established environmental magnetic proxy parameters on fluvial sediments, with the aim to trace geological and human-induced processes in the complex Seine river drainage system in northern France. We seek to identify environmental fingerprints of mechanical and chemical weathering processes, the regional distribution of the suspended material, and changes in the balance of natural input versus anthropogenic pollution. In order to reach these goals, we applied a combination of rock magnetic and advanced scanning electron microscopic techniques on a large number of sediment trap samples. Generally, we observe an increase in magnetic concentration coupled with a coarsening in magnetic grain size downstream of the Seine river system. Furthermore, the dominant magnetomineralogy changes from high-coercivity minerals upstream in more rural areas to magnetite-dominated assemblages downstream. Each river (segment) shows its specific trend line depending on regional initial input, weathering conditions, drainage area, and potential pollution sources. One major outcome of this study is the observed significant correlation between anthropogenic antimony-rich iron oxide particles and the magnetic concentration. This shows the potential of magnetic remanence measurements as proxy parameters for specific heavy metal pollution concentrations. Hence, the environmental magnetic study presented herein serves to identify major trends as well as local particularities and leads to quantitative analyses of the contributions of individual tributaries in the Seine river system.

1. Introduction

[2] Major fluvial systems are important carriers of suspended sediment load from source areas to the oceans. They usually contain a complex mixture of weathered soils or source rocks, atmospheric dust, urban and industrial wastewaters, agricultural input and other natural or anthropogenic particles. Once the material enters the river, it may be either deposited in situ or transported further downstream depending on the nature of the particle, its grain size and the current strengths in the stream. This input of material may occur at any point of the river system: continuously or periodically, on a local scale or over a wider geographical area. Numerous alteration processes of the primary input can take place along the river system, such as geochemical oxidation or reduction of the particles, as well as clustering or mechanical abrasion. The combination of all these processes results in a highly complex and sensible fluvial system, which may have important impacts on, for example, water quality, ecosystems, or erosion or depositional behavior along the river itself or in its delta area [*Turner and Rabalais*, 1991].

[3] Eroded sediment, nutrients, organic matter, and anthropogenic particles (e.g., heavy metals) are primarily transported as suspended particle load and their characterization and quantification may improve our understanding of fluvial geochemical and geodynamical processes. The suspended particle load is in turn the ideal material, unaffected by any depositional induced diagenetic alterations, to identify sediment sources including those of anthropogenic pollutions.

[4] The magnetic fraction of a sediment holds key information (mineralogy, grain size, concentration) regarding the sediments geological history, such as its provenance and its response to climate and the environment. Moreover, characterizing the properties of the magnetic mineral assemblage can be easily determined using standard rock and environmental magnetic methods [e.g., *Thompson and Oldfield*, 1986; *Maher and Thompson*, 1999; *Evans and Heller*, 2003, and references therein]. Previously published magnetic studies on fluvial sediments are few and limited to room temperature magnetic susceptibility and/or remanence analyses [e.g., *Yang et al.*, 2007; *Hatfield and Maher*, 2008]. Furthermore, the targeted sediments, from river beds or connected lakes, are subject to depositional and postdepositional alteration processes which can obliterate (or mask) the sediment's primary origins. The multidisciplinary approach taken here, on the magnetic fraction suspended in the water column, shows the potential to detect multiparameter changes in the particle load along the Seine river system in northern France.

[5] The Seine river watershed (Figure 1) spans about 67500 km^2 [*Meybeck et al.*, 1998; *Tessier and Bonté*, 2002] and is widely covered by Quaternary loess and fluvial deposits. The main part of the basin, outside of Paris and its agglomerations, is dominated by extensive farming and natural vegetation. Additionally, the Seine river basin encompasses all major contamination sources associated with modern industrialized society, such as a high population density, heavy industry, river channeling, and reservoir constructions [*Horowitz et al.*, 1999]. From headwaters to the city of Paris, the Seine river drains the plateaus and tablelands of Jurassic limestones and terrigenous sediments, Lower Cretaceous sands and marls, Upper Cretaceous chalks, and Tertiary limestones and marls. In the southern part of the basin, the Yonne river drains Hercynian gneissic, granitic, and rhyolitic rocks before flowing into the Seine [*Roy et al.*, 1999].

[6] The aim of this study is to identify environmental fingerprints of mechanical and chemical weathering processes, the regional distribution of the suspended material, the influence of fluvial transport mechanisms, and changes in the balance
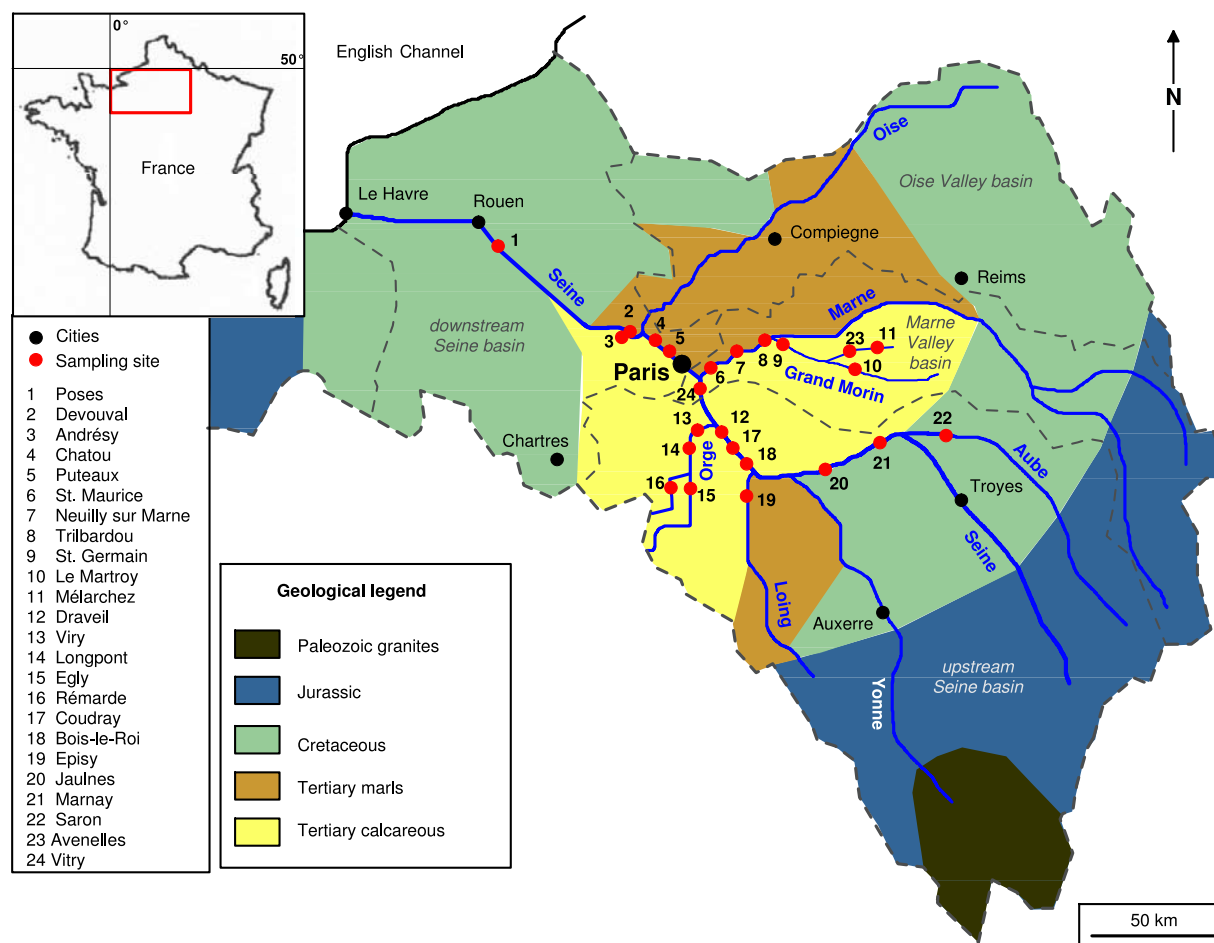
Figure 1. Schematic geological map (interpolated from *Roy et al.* [1999]) of the main lithological units in the Seine river drainage area (outer dashed gray line) in northern France, showing the major cities in the area (black filled dots) and the chosen sampling sites (red filled dots). Site numbers and corresponding site names are given in the legend. Inner dashed gray lines mark the individual drainage areas of the respective rivers. For color coding please see geological legend.

of natural input versus anthropogenic pollution. To reach these goals, we took advantage of a systematic large-area sampling campaign of suspended material by *Tessier* [2003] covering the Seine river watershed. The small sample masses of the available suspended material are well adapted to environmental magnetic analyses, such as room temperature magnetic hysteresis and low-temperature remanence measurements. These specific qualitative magnetic measurements were combined with a powerful absolute quantitative scanning electron microscope (SEM) technique [*Robin et al.*, 1991]. This allows for the chemical classification of each identified magnetic particle type. Our multidisciplinary approach provided the means to improve our understanding of the hydrological and sedimentary processes in major river systems. This in turn is critical to our comprehension of the relationship

between geology and complex fluvial systems and their impacts on the systems' ecology.

2. Material and Methods

2.1. Sampled Suspended Particle Load

[7] The suspended sediment material originates from a sampling campaign performed in 2001 by *Tessier* [2003] using sediment traps of ~2 L in volume. These were installed at various locations in the central part of the major rivers Seine and Marne in northern France, or near the confluence of their respective tributary streams. Figure 1 shows the drainage area of the Seine river system including all 24 sediment trap sites selected for this study. These sites are distributed along three

Table 1. Sample Sites and Numbers, Respective River, Sampling Date, Drainage Area, and Distance to the Most Downstream Seine Site Poses

Site Number	Sample Site	River	Date of Sampling[a]	Drainage Area[a] (km²)	Distance From Poses[a] (km)
1	Poses	Seine	20 Jul 2000	64,940	0
2	Denouval	Seine	26 Jul 1999	61,755	102
3	Andrésy	Seine	19 Jul 1999	61,755	102
4	Chatou	Seine	11 Jul 2001	44,558	144
5	Puteaux	Seine	18 Jul 2001	44,057	174
6	St. Maurice	Marne	18 Jul 2001	12,832	188
7	Neuilly s. M.	Marne	18 Jul 2001	12,722	205
8	Trilbardou	Marne	31 Jul 2001	12,242	246
9	St. Germain	Grand Morin	16 Jul 2001	1,202	249
10	Le Martroy	Grand Morin	16 Jul 2001	617	292
11	Mélarchez	Mélarchez/Gd. Mo.	16 Jul 2001	16	298
12	Draveil	Seine	18 Jul 2001	28,664	202
13	Viry	Orge	25 Jul 2001	937	201
14	Longpont	Orge	18 Jul 2001	615	209
15	Egly	Orge	17 Jul 2001	228	217
16	Rémarde	Rémarde/Orge	17 Jul 2001	287	220
17	Coudray	Seine	17 Jul 2001	26,589	219
18	Bois-le-Roi	Seine	25 Jul 2001	25,686	242
19	Episy	Loing	25 Jul 2001	3,946	270
20	Jaulnes	Seine	31 Jul 2001	9,596	305
21	Marnay	Seine	17 Jul 2001	8,900	350
22	Saron	Aube	31 Jul 2001	4,592	371
23	Avenelles	Grand Morin	4 Jul 2001	45	291
24	Vitry	Seine	9 Aug 2001	30,718	190

[a] Data taken from *Tessier* [2003].

profiles from rural areas to more industrialized or urbanized areas, including the megacity of Paris.

[8] Profile 1 (sites 1 to 11, including 23) starts in the Grand Morin tributary northeast of Paris, flows into the river Marne, confluences with the Seine between Vitry (site 24) and Puteaux (site 5), and runs downstream to Poses (site 1). All sites of profile 2 (sites 1–5, 12, 17, 18, 20–22, and 24) are situated within the Seine river with the exception of site 22 at the head of the profile, located within the Aube tributary. The final segment along the Seine between Puteaux (site 5) and Poses (site 1) is common to profiles 1 and 2. Profile 3 (sites 13–16) runs down the Orge tributary southeast of Paris and confluences with the Seine immediately downstream from Draveil (site 12).

[9] All investigated samples (Table 1) were taken within the narrow time span of a few days in July 2001 during which weather conditions had been stable [*Tessier and Bonté*, 2002]. The suspended material was freeze dried in the laboratory immediately after sampling, to prevent any chemical alteration. For further information on instrumentation and sampling details the reader is referred to *Tessier and Bonté* [2002] and *Tessier* [2003]. Seasonal climatic changes strongly influence the

pH value in the river, the water volume/level and the predominant input mechanisms. Summer conditions are characterized by a rather oxic water column, medium to low flow rate, and atmospheric dust and periodical summer rainstorms as the dominant natural sediment input.

2.2. Rock Magnetic Methods

[10] Room temperature magnetic hysteresis loops and backfield remanence were measured on dry bulk sediment (1 to 7 mg), using an alternating gradient force magnetometer (AGFM 2900) at the LSCE. Hysteresis loop parameters, saturation magnetization M_s, remanent saturation magnetization M_{rs}, coercive force B_c and coercivity of remanence B_{cr} were derived from high field (diamagnetic and paramagnetic) slope corrected loops. Loops were determined in both 0.3 and 1 T maximum fields.

[11] To estimate concentrations of high-coercivity components from the hard isothermal remanent magnetization (HIRM), saturation isothermal remanent magnetization (SIRM) was acquired in 1 T after the low-field (0.3 T) hysteresis loop measurements. Subsequently, a −0.3 T backfield remanence measurement was applied, which was used to calculate the HIRM following the method

described by *Stoner et al.* [1996]. The HIRM is defined as $(SIRM_{1T} + IRM_{-0.3T})/2$ and is referred to as $HIRM_{-0.3T}$.

[12] Since one of the major questions in this study was the distinction of anthropogenic versus natural magnetic particles along the investigated river profiles, we chose on purpose to focus on the 0.3 T hysteresis results, because they are representative of the soft magnetic mineral fraction. It is known from other environmental magnetic studies [e.g., *Georgeaud et al.*, 1997; *Jordanova et al.*, 2004; *Chaparro et al.*, 2004], that anthropogenic pollution is mainly represented in this soft (magnetite-dominated) fraction, which is usually sufficiently saturated at applied maximum fields of 0.3 T.

[13] High−coercivity minerals, such as goethite and hematite, are not or only insufficiently saturated in such applied fields of 0.3 T. We take advantage of this, because the 0.3 T loops are therefore a good measure to derive the magnetic concentration of the soft components. Using the 1 T hysteresis loops to quantify the magnetic concentration of soft components would strongly bias the results in the presence of high−coercivity minerals. To check also for the change in magnetomineralogy we calculated the $HIRM_{-0.3T}$ parameter as further discussed in section 3.1.2.

[14] Low−temperature magnetic measurements were performed on dry bulk sediments using a Quantum Design Magnetic Properties Measurement System (MPMS) at the IPGP (France) and at the University of Bremen (Germany). The sample weight varied between 20 to 250 mg, for absolute comparison all remanence curves are weight normalized. Details on sample preparation and instrumentation are given by *Frederichs et al.* [2003]. Room temperature saturation isothermal remanent magnetization cycles (RT−SIRM) were monitored between 300 and 5 K using 5 K increments. The cooling−warming remanence cycles were measured in zero field after the samples acquired their remanence at room temperature in an applied field of 2.5 T or 5 T.

2.3. Scanning Electron Microscopy Analytical Method

[15] For SEM analyses, magnetic extracts were prepared using the method described by *Robin and Molina* [2006]. Such concentrates are biased toward strongly ferrimagnetic mineral phases [e.g., *Franke et al.*, 2007a] and very often, weaker magnetic minerals, such as antiferromagnetic goe-

thite and hematite, are not fully extracted. Nevertheless, the magnetic extracts are easily obtainable and relatively pure; they give a reasonable overview on the variety of the present mineral phases. As a mean of quality control, SEM analyses were also performed for a few heavy liquid separates from selected sites following the protocol by *Franke et al.* [2007a]. As outlined by the authors, this density based concentration method does not discriminate between any type of material within the heavy mineral fraction ($\rho \geq 3.0$). The SEM analyses of both types of concentrates were compared and resulted in similar proportions for all magnetic phases identified in the SEM. Therefore, even though the simpler extraction method biases strongly magnetic minerals, for the samples of this study the extraction is representative of the total iron oxide assemblage.

[16] The separated particles were flushed into a beaker and ultrasonically dispersed in ethanol before they were recovered on a 1 μm nuclepore filter. The filter was dried in air, stuck on a standard SEM stub and coated with a thin layer of carbon. A JEOL 840 SEM at the LSCE associated with an energy Princeton Gamma Tech X-ray dispersive spectrometer (EDS) was used for determining the chemical composition.

[17] The well-dispersed particles on the filter were analyzed using a SEM/EDS search routine called Automated Chemical Classification (ACC) that was previously developed by *Robin et al.* [1991] for the analysis of Ni-rich spinel crystals. Individual particles present on the filter are identified, counted and virtually sorted by their size, shape and chemical composition. The particle classification technique can be adjusted as defined by the user for the analysis of many other mineral phases, such as shown for barite containing samples [*Robin et al.*, 2003] or as applied in this study on iron oxide and sulphide particles. The ACC technique allows for absolute quantifications of the different identified minerals with respect to a grain size of ≥ 0.5 μm. For further instrumental details see also *Robin and Molina* [2006].

3. Environmental Magnetic Analyses

3.1. Room Temperature Magnetic Hysteresis

3.1.1. Concentration of Magnetic Particles

[18] Mass-specific saturation magnetization M_s is used here as a concentration-dependent parameter
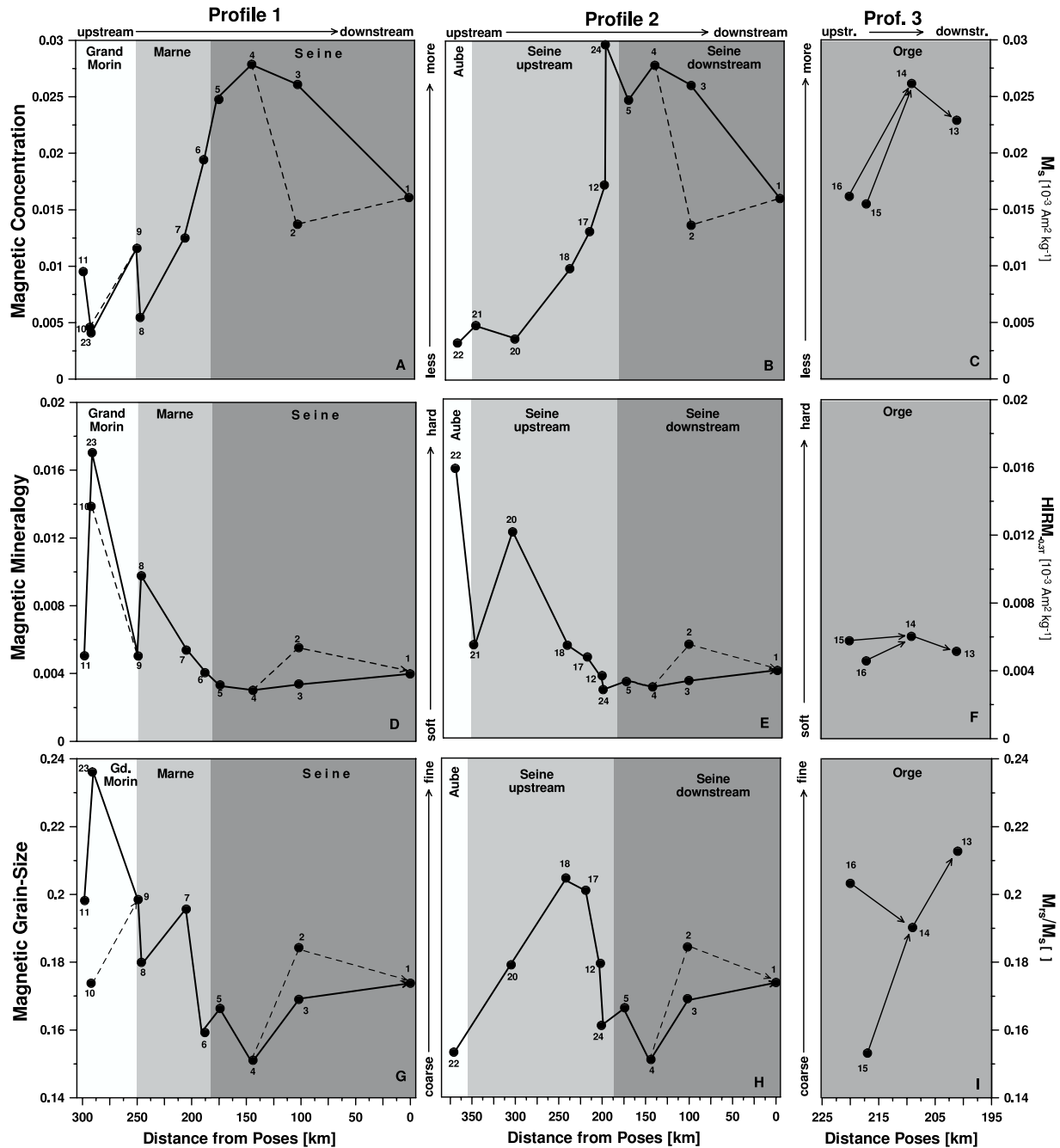
Figure 2. Results from rock magnetic analyses for the three transects along the Grand Morin-Marne-Seine (profile 1), the Aube-Seine (profile 2), and the Orge (profile 3). (a–c) The magnetic concentration parameter M_s, (d–f) the magnetomineralogy parameter $HIRM_{-0.3T}$, and (g–i) the magnetic grain size parameter M_{rs}/M_s. Numbers on data points correspond to sample sites introduced in Figure 1. Changes in gray tones indicate the downstream confluence into the subsequent river. The black line displays the major river profile, and dashed lines indicate parallel river flow or inflow from smaller rivers. For profile 3, arrows give the general flow direction from site to site. Note that sites 16 and 15 are not situated on the same river but are quasi-parallel sites.

(see Table 2). As shown in Figure 2a along profile 1, M_s starts to decrease along the Grand Morin river northeast of Paris. Very close to the confluence with the Marne (at site 9 = St. Germain) the magnetic concentration shows similar values as in the beginning of the profile. Between St. Germain (site 9) and Trilbardou (site 8) the concentration drops again to values comparable to those at site 10 and 23. After the confluence with the Marne (site 8 = Trilbardou), a steep increasing trend in the

Table 2. Rock Magnetic Parameters Derived From Room Temperature Magnetic Hysteresis Measurements[a]

Sample Site	Site Number	M_s (10^{-3} Am^2 kg^{-1})	M_{rs} (10^{-3} Am^2 kg^{-1})	B_c (mT)	B_{cr} (mT)	HIRM$_{-0.3T}$ (10^{-3} Am^2 kg^{-1})
Poses	1	0.0161	0.0028	3.84	13.02	0.0042
Denouval	2	0.0137	0.0025	5.51	21.12	0.0055
Andrésy	3	0.0261	0.0044	5.00	18.03	0.0034
Chatou	4	0.0279	0.0042	2.46	8.21	0.0030
Puteaux	5	0.0248	0.0041	2.38	9.90	0.0033
St. Maurice	6	0.0194	0.0031	3.60	14.14	0.0041
Neuilly	7	0.0125	0.0024	1.25	4.49	0.0054
Trilbardou	8	0.0055	0.0010	4.71	15.11	0.0098
St. Germain	9	0.0116	0.0023	3.97	14.02	0.0050
Le Martroy	10	0.0046	0.0008	4.16	17.53	0.0139
Mélarchez	11	0.0095	0.0019	2.52	11.19	0.0050
Avenelles	23	0.0041	0.0010	5.85	22.09	0.0170
Vitry	24	0.0297	0.0048	3.43	12.90	0.0028
Draveil	12	0.0173	0.0031	2.79	9.65	0.0037
Viry 45	13	0.0229	0.0049	1.64	4.80	0.0059
Longpont	14	0.0262	0.0050	1.63	5.89	0.0042
Egly 44	15	0.0155	0.0024	1.62	6.03	0.0050
Rémarde	16	0.0162	0.0033	2.21	7.04	0.0042
Coudray	17	0.0131	0.0026	4.97	16.71	0.0048
Bois-le-Roi	18	0.0099	0.0020	5.06	15.44	0.0055
Episy	19	0.0106	0.0019	1.77	5.38	0.0053
Jaulnes	20	0.0036	0.0007	3.64	12.95	0.0122
Marnay	21	0.0048	0.0017	2.15	6.71	0.0055
Saron	22	0.0033	0.0005	5.38	16.42	0.0159

[a] Mass-specific saturation magnetization M_s, mass-specific remanent saturation magnetization M_{rs}, coercive force B_c, coercivity of remanence B_{cr}, and the calculated HIRM$_{-0.3T}$.

magnetic concentration is observed. The general increasing trend continues with a lower slope after the confluence of the Marne with the Seine until site 4 at Chatou. The last sites analyzed along the profile (until Poses = site 1) have a lower magnetic concentration and therefore suggest a possible decrease between Andrésy and Poses. Along the second profile, no initial decreasing trend could be detected in the magnetic concentration (Figure 2b). Instead we observe a steady increase in concentration of the magnetic fraction along the Aube and the Seine river just until Chatou (site 4). A small drop is observed between Vitry (site 24) and Puteaux (site 5), which might be due to the fact that between those two sites, the Marne confluences with the Seine.

[19] The two relatively close sampling sites 2 (Denouval) and 3 (Andrésy) exhibit significantly different characteristics. They are located within the river Seine northwest of Paris after its confluence with the Oise river. In this area, a chain of several islands (Ile de la Derivation, Ile d'en Bas, Ile de Devant, Ile Nancy) divides the Seine stream into two separate channels. The right hand side (where site 2 is located) is dominated by the inflow of Oise water masses, while the left hand side (site 3) belongs to the regular course of the Seine. Note that at Andrésy the Seine also receives the efflu-

ences of the wastewater plant in Achères, which treats the majority of the downstream Seine liquid waste (including Paris). It therefore seems that the different values observed for site 2 represent to a wide extent the lower concentration of suspended material coming from the Oise inflow, which is not yet mixed here with the suspended load of the Seine.

[20] The magnetic concentration along the Orge river (profile 3) is shown in Figure 2c. A strong increase in M_s can be seen between the two upstream sites 16 (Rémarde) and 15 (Egly) and the two downstream sites 14 (Longpont) and 13 (Viry). Site 16 is a sampling station in a smaller tributary stream of the Orge (called Rémarde), whereas site 15 is situated directly in the course of the Orge river. The Rémarde stream joins the Orge a few kilometers northeast of Egly. Therefore site 16 and site 15 are parallel sampling stations, both converging 6 km upstream of Longpont. The observed magnetic concentration values at Rémarde and Egly are comparable with those detected for the downstream Marne (e.g., at Neuilly = site 7 or St. Maurice = site 6; compare Figure 2a) or the upstream Seine (e.g., at Draveil = site 12; compare Figure 2b). Over the distance of only 20 km the concentration values along the

Orge increase steeply. Similarly high values were otherwise only observed for the downstream sites of the Seine at, e.g., Puteaux or Chatou (sites 5 and 4).

3.1.2. Mineralogy of the Magnetic Assemblage

[21] The hard isothermal remanent magnetization (HIRM) is a measure of the dominating mineralogy within a magnetic assemblage [*Stoner et al.*, 1996] and can be used to describe relative changes in the concentration of high-coercivity material [e.g., *Dunlop and Özdemir*, 1997].

[22] Profile 1 shows, with exception of site 11, a downstream trend along the Grand Morin from rather high concentrations of high-coercivity components at the upstream sites Le Martroy and Avenelles (site 10 and 23) to lower concentrations of high-coercivity phases further downstream at the confluence with the Marne (site 9, Figure 2d). Here we observe a clear decrease of $HIRM_{-0.3T}$ values up to the junction with the Seine at St. Maurice (site 6). Along the final segment of the Seine, $HIRM_{-0.3T}$ values are relatively constant and low.

[23] Figure 2e shows the evolution of the $HIRM_{-0.3T}$ along profile 2. Here we can observe the same clear bisection between the Aube-Seine upstream and the Seine downstream trench. Along the Aube and upstream Seine transect, a progressive decrease in the concentration of high-coercivity material is detected, with exception for site 21. The observed values for this upstream Seine river segment are very similar to those of the Marne sites (compare Figures 2d and 2e). For the sites located downstream with respect to Vitry (site 24) the data points are the same as for profile 1 and exhibit therefore the same constant trend. Along the Orge profile 3 (Figure 2f), all sample sites show similar values, more or less comparable to those of the upstream Seine at Bois-le-Roi and Coudray (sites 18 and 17), typical for a magnetite-dominated particle assemblage.

3.1.3. Magnetic Grain Size

[24] The average grain size of a magnetic assemblage can be characterized by the grain size–dependent parameter M_{rs}/M_s derived from room temperature hysteresis measurements [e.g., *Dunlop and Özdemir*, 1997]. Strictly speaking, this assumption is only valid for monomineralogic magnetic assemblages. Since here we use the 0.3 T hysteresis data, only the soft ferrimagnetic fraction should be represented by our grain size parameter.

[25] Profile 1 (Figure 2g) starts with M_{rs}/M_s values around 0.20 in the upstream Grand Morin (site 11) and shows a fining trend at Avenelles (site 23) before it drops again to a comparable coarser value around 0.19. At the junction of the Grand Morin and the Marne, the values obtained for both rivers are relatively similar, but further along the Marne the M_{rs}/M_s ratio decreases and shows a clear coarsening trend, which continues also along the Seine until Chatou (site 4). Once the Seine passed the Paris megacity, the M_{rs}/M_s values increase again and therefore show a slight fining trend in average magnetic grain size for this last Seine downstream segment of profile 1 and 2. The magnetic grain size along profile 2 (Figure 2h) shows a fining trend for the Aube and upstream Seine sites until site 18 (Bois-le-Roi). Site 21 shows an exceptional fine M_{rs}/M_s value (0.35, not plotted in the same diagram because of scaling problems). With respect to site 21 we refer to Figure 3a, which will be briefly discuss in the following paragraph. The fining trend changes between Bois-le-Roi and Coudray (sites 18 and 17) into a clear coarsening trend, which continues up to Chatou (site 4). Downstream from site 4 the M_{rs}/M_s values stay more or less constant at about 0.17. Along the Orge profile 3, a general fining trend can be observed (Figure 2i), with the exception for site 16 (Rémarde), which shows a fine magneto-granulometry starting value. Comparing the different trends, it appears that the finest magnetic fraction is most of the time associated with the hardest magnetic mineralogy and vice versa.

[26] The observed magnetic domain states for all investigated samples are shown river-wise in Figure 3a in a Day plot [*Day et al.*, 1977; *Dunlop*, 2002]. Figures 3b and 3c show a representative example for a uncorrected loop of the 0.3 T and 1 T hysteresis measurement, which points out the magnetite dominance of the samples. All samples have a relatively coarse magnetic assemblage falling into the field of coarse pseudo–single domain (PSD) (magnetite) particles. The coarsest PSD samples originate from the upstream Grand Morin sites and close to the Paris area, the finest identified PSD samples stem from the upstream Aube-Seine sites.

3.2. Low-Temperature Magnetic Remanence

[27] Figures 4 and 5 show RT-SIRM cycles of 14 selected samples for low-temperature (LT) magnetic measurements. Each site depicts an individual regional signal depending on the concentration, mineralogy, and grain size of its magnetic fraction. The initial mass normalized saturation remanences ac-
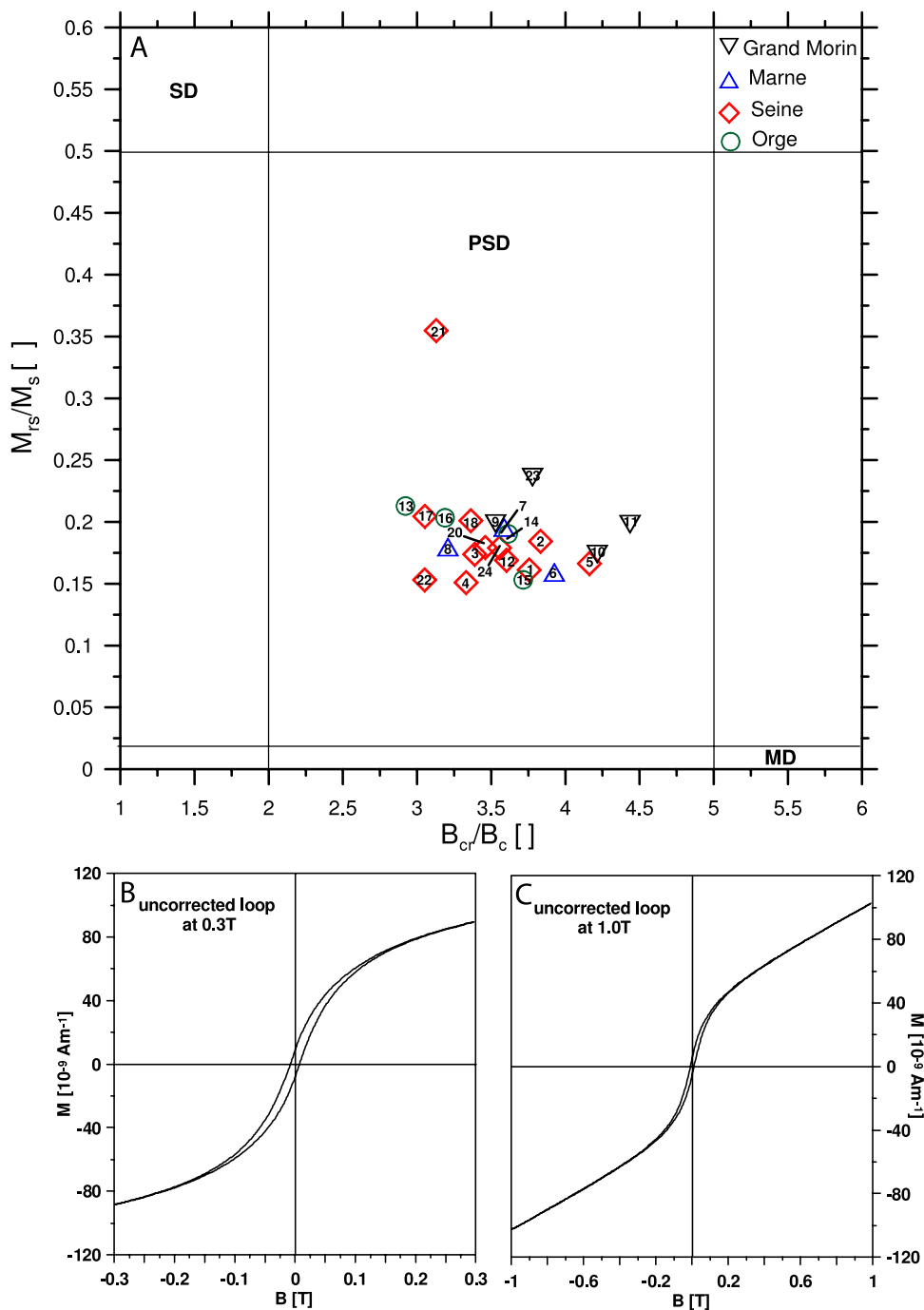
Figure 3. (a) Hysteresis loop parameters plotted river-wise in a "Day diagram" [*Day et al.*, 1977; *Dunlop*, 2002]. Numbering corresponds to sample sites: Grand Morin (black inversed triangles), Marne (blue triangles), Seine (red diamonds), and Orge (green circles). SD, single domain; PSD, pseudo−single domain; MD, multidomain. (b) Representative uncorrected hysteresis loop measured at 0.3 T maximum applied field and (c) respective hysteresis loop measured at 1 T maximum applied field.

quired in 2.5 T (IPGP) or 5 T (Bremen), are generally lower in the upstream sites and increase continuously downstream (Table 3). This is in agreement with the observed downstream increase in magnetic concentration (compare Figures 2a–2c). In addition, the total remanence loss after a complete cooling-warming cycle increases systematically from upstream to downstream sites. As magnetite grain size increases, total remanence lost upon cycling of a RT-SIRM below T_V and back also increases [*Özdemir et al.*, 2002]. Therefore, RT-SIRM experiments show a downstream increase in magnetite particle grain size.
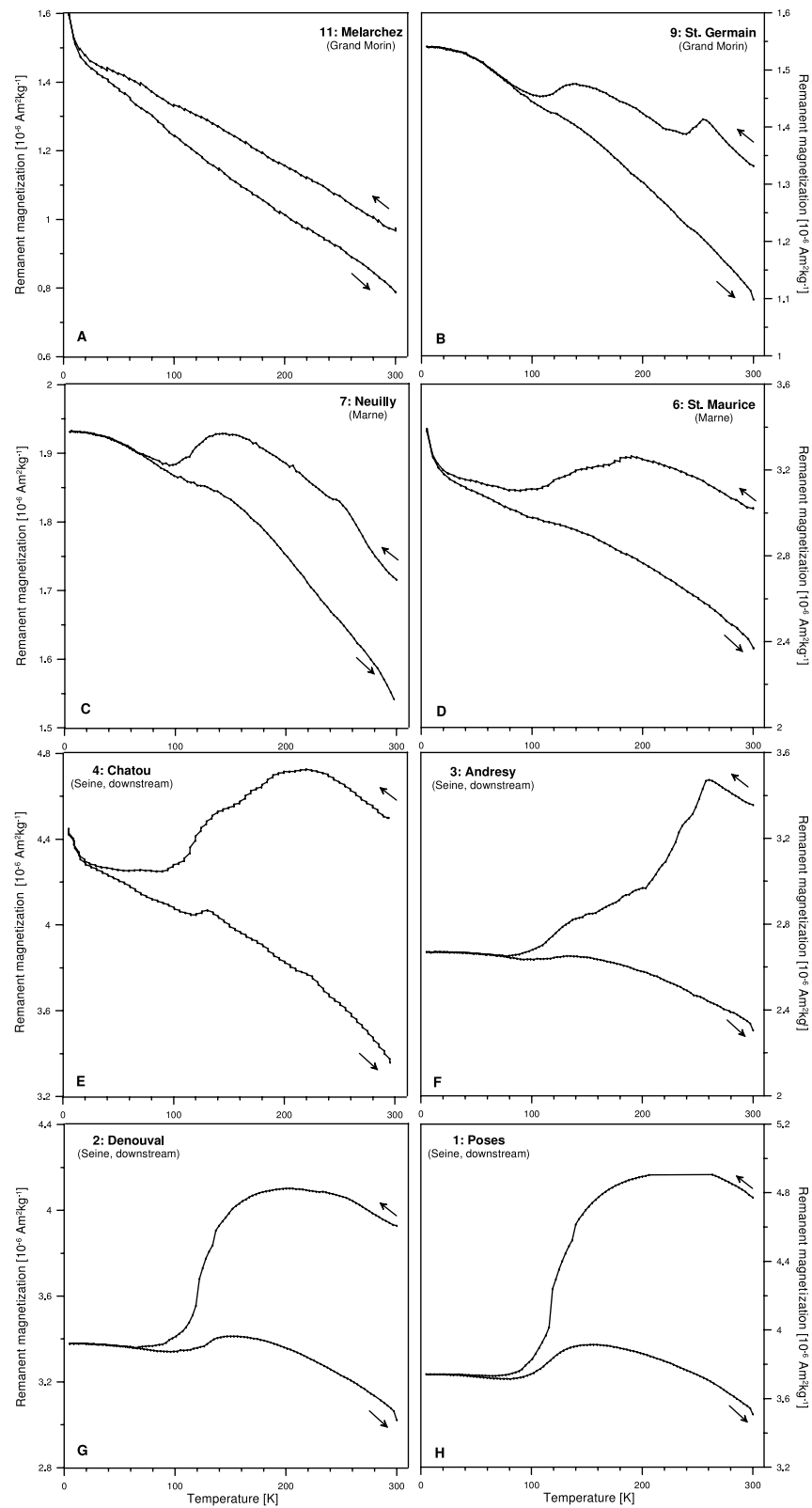
Figure 4. Mass-normalized RT-SIRM cycles for selected bulk sediment samples from the Grand Morin, Marne, and downstream Seine sites (along profile 1). Small arrows indicate the direction of the cooling-warming branches of the remanence curves. (a) Site 11, Mélarchez, Grand Morin; (b) site 9, St. Germain, Grand Morin; (c) site 7, Neuilly, Marne; (d) site 6, St. Maurice, Marne; (e) site 4, Chatou, Seine downstream; (f) site 3, Andresy, Seine downstream; (g) site 2, Denouval, Seine downstream; and (h) site 1, Poses, Seine downstream.
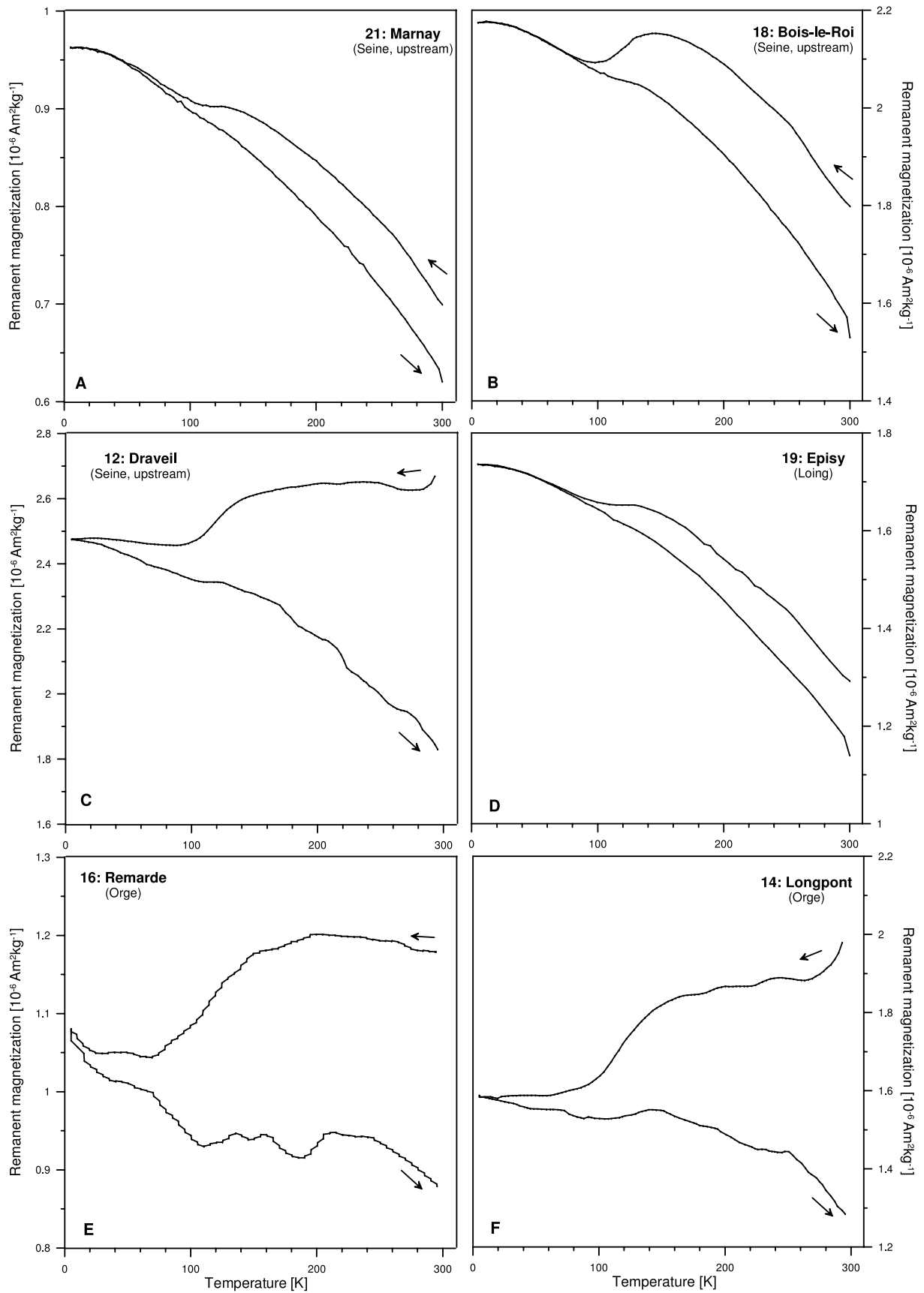
Figure 5

Table 3. Initial and Final Weight Normalized Remanence Values as Well as Calculated Remanence Loss Derived From the RT-SIRM Cycles for All Selected Low-Temperature Magnetic Measurements[a]

Site Number	Sample Site	Initial Remanence $(10^{-6}$ Am^2 kg$^{-1})$	Final Remanence $(10^{-6}$ Am^2 kg$^{-1})$	Remanence Loss (%)	Detected Transitions/Features
1	Poses	4.77	3.51	26.42	T_V
2	Denouval	3.93	3.02	23.16	T_V
3	Andrésy	3.36	2.31	31.25	$T_V., T_M$
4	Chatou	4.51	3.32	26.39	$T_V,$
6	St. Maurice	3.02	2.37	21.53	$T_V,$
7	Neuilly	1.72	1.51	12.21	$T_V, S_G, (T_M)$
9	St. Germain	1.33	1.10	17.29	T_V, T_M, S_G
11	Mélarchez	0.97	0.79	18.56	S_G
12	Draveil	2.73	1.80	34.07	$T_V,$
14	Longpont	2.05	1.27	38.05	$T_V,$
16	Rémarde	1.18	0.87	26.27	T_V
18	Bois-le-Roi	1.80	1.53	15.00	T_V, S_G
19	Episy	1.29	1.14	11.63	$T_V, S_G, (T_M)$
21	Marnay	0.70	0.62	11.43	T_V, S_G

[a] The sixth column gives a summary on the low-temperature (LT) magnetic transitions. Mineral discriminative LT features are as follows: T_V, Verwey transition; T_M, Morin transition; S_G, goethite indicative LT slope. For further explanations see section 3.2.

This observation agrees with observed downstream magnetic softening and coarsening of magnetic granulometry trends based on hysteresis loop parameters (section 3.1 and Figures 2d–2i).

[28] The third important observation is a change in the magnetomineralogy from goethite-hematite and Ti-rich iron oxide dominated curves for the upstream sites to magnetite dominated signals for the downstream sites. This is illustrated by the continuous reversible positive slope of remanence with decreasing temperature (see, e.g., Figure 4a, Mélarchez), which is specific for the low-temperature behavior of goethite [*Lowrie and Heller*, 1982; *Dekkers*, 1989], and the observed Morin transition (T_M) (Figure 4b, St. Germain; Figure 4f, Andrésy) between 240 and 260 K unique to hematite [*Morin*, 1950; *Morrish*, 1995].

[29] Almost all samples show the presence of magnetite, expressed through the Verwey transition (T_V) situated between 120 and 100 K [*Verwey*, 1935; *Özdemir et al.*, 2002; *Özdemir and Dunlop*, 2003; *Kosterov*, 2003], except for site 11 (Mélarchez, Figure 4a). The T_V temperature for the downstream Seine samples (sites 4 to 1, Figures 4e–4h) indicates near stoichiometric magnetite values of 120 K, whereas the upstream Seine samples show slightly lower temperatures around 110 K. The shift toward lower T_V temperatures might be due to slightly oxidized magnetite particles [e.g., *Özdemir et al.*, 1993]. Lower T_V temperatures are observed in the

samples from the Marne, Orge, and Grand Morin rivers (see Figures 4b–4d, 5e, and 5f). For samples with Ti-Fe oxides ($Fe_{2-x}Ti_xO_4$) and a Ti content of $x \geq 0.04$, the Verwey transition is suppressed [*Kakol et al.*, 1994], such as seen in site 11 (Mélarchez; Figure 4a) or site 19 (Episy, Loing river; Figure 5d). The individual shape of the RT-SIRM curves therefore depends strongly on the Fe-Ti composition of the magnetic assemblage and the proportion of high(er)-coercivity minerals in the samples [e.g., *Lagroix et al.*, 2004; *Franke et al.*, 2007a; *Dillon and Franke*, 2009].

[30] In the downstream Seine sites, goethite type behavior (reversible increasing remanence with decreasing temperature) is no longer observed in the RT-SIRM curves. However, at Andrésy (site 3) hematite's Morin transition is detected at 260 K. The source of this local "hematite peak" is most likely the Achères wastewater plant (main treatment plant for Paris) which discharges into the Seine here. Hematite is not detected in the parallel site at Denouval shadowed from the wastewater treatment plant by the island, nor in the other downstream sites. The RT-SIRM curve of Andrésy shows furthermore a clear continuous remanence decrease in two steps, first between 260 and 200 K and second between 200 K and the Verwey transition. Similar curves were published for natural mixtures of titanomagnetite and titanohematite by, e.g., *Garming et al.* [2007].

Figure 5. Mass-normalized RT-SIRM cycles for selected bulk sediment samples from the upstream Seine (along profile 2), Orge (profile 3), and Loing river. Small arrows indicate the direction of the cooling-warming branches of the remanence curves. (a) Site 21, Marnay, Seine upstream; (b) site 18, Bois-le-Roi, Seine upstream; (c) site 12, Draveil, Seine upstream; (d) site 19, Episy, Loing; (e) site 16, Remarde, Orge; and (f) site 14, Longpont, Orge.

Table 4. Results From SEM/ACC Analyses

Sample Site	Site Number	Pure Iron Oxides (%)	Mg-Rich Iron Oxides (%)	Ti-Rich Iron Oxides (%)	Cr-Rich Iron Oxides (%)	Mn-Rich Iron Oxides (%)	Sb-Rich Iron Oxide (%)	Total Particles (mg^{-1})
Poses	1	78.6	8.5	5.4	2.5	3.1	2.0	14,488
Denouval	2	77.0	8.6	7.3	0.8	2.0	4.2	5,402
Andrésy	3	76.7	8.6	5.7	3.4	3.7	2.0	5,238
Chatou	4	72.4	7.1	6.6	1.8	2.3	9.8	13,437
Puteau	5	71.0	10.5	6.5	2.5	3.6	6.0	3,104
St Maurice	6	67.9	9.4	12.1	2.4	3.4	4.8	13,149
Neuilly	7	66.5	7.0	12.7	4.1	5.6	4.0	4,164
Trilbardou	8	64.5	6.3	16.8	2.5	8.8	1.2	3,520
St Germain	9	65.9	8.6	14.4	2.4	4.7	4.0	3,533
Le Martroy	10	55.3	5.7	18.5	4.8	12.8	3.0	1,210
Mélarchez	11	31.3	7.5	52.6	2.6	4.9	1.1	7,389
Draveil	12	77.5	6.8	7.7	1.1	2.0	4.9	3,689
Viry	13	71.2	8.2	8.8	1.3	4.0	6.5	7,668
Longpont	14	68.9	13.9	8.2	1.4	2.4	5.3	2,184
Egly	15	56.3	10.0	26.1	2.3	3.7	1.7	2,624
Rémarde	16	73.2	6.2	13.1	1.1	3.8	2.5	1,213
Coudray	17	79.5	3.9	8.8	1.6	3.0	3.2	9,026
Bois-le-Roi	18	76.4	4.1	11.0	2.7	3.8	2.0	4,309
Episy	19	65.6	6.3	20.9	2.1	3.0	2.2	2,781
Jaulnes	20	73.0	6.5	11.4	2.2	4.0	2.8	3,265
Marnay	21	67.8	6.6	17.8	2.7	3.7	1.3	1,093
Saron	22	69.5	2.9	19.8	1.7	2.2	3.9	1,360
Avenelles	23	47.1	9.5	31.6	3.3	6.9	1.6	1,016
Vitry	24	74.2	7.6	7.4	1.6	2.5	6.7	9,704

[31] The LT results for the two samples from the Orge profile 3 (Rémarde and Longpont) show relatively similar RT-SIRM curves, both depicting "magnetite-like" curve shapes with a T_V around 110 K and relatively important remanence loss values of 26% and 38%, respectively. These findings agree with the results from the room temperature hysteresis measurements identifying a soft magnetomineralogy with a relatively coarse grain size of the magnetic fraction (compare to Figures 2f and 2i). Site 12 (Draveil, Figure 5c), situated near and downstream of the Orge's confluence with the Seine resembles more the Orge river sites than upstream Seine River sites. This suggests that the water masses from the Orge, although originating from a relatively small river and fed by a smaller catchment area, have an important impact on the Seine particle load and its (magnetic) signal.

4. SEM Automated Chemical Classification

[32] The ACC results allow the definition of six principal particle classes, which are (1) pure iron oxides, (2) Ti-rich iron oxides, (3) Sb-rich iron oxides, (4) Mg-rich iron oxides, (5) Cr-rich iron oxides, and (6) Mn-rich iron oxides. The total proportions of each particle class per sample site can be found in Table 4. In the following we will focus on the above-defined particle classes and briefly describe their main characteristics.

[33] Particle class 1 consists of pure iron oxide and oxy-hydroxide minerals, i.e., containing less than 0.5 wt % of Ti, Sb, Mg, Cr, and Mn. Visual spot checks show that this particle class contains several different particle types, such as detrital iron oxides (Figure 6a) next to iron oxide spherules (Figure 6c, grain on the right), in a range from a few hundred microns to submicron scale. Magnetite (Fe_3O_4) is clearly the dominating mineral phase, since we used a magnetic extraction method which favors these strongly ferrimagnetic particles. However, we cannot exclude the contribution of hematite (Fe_2O_3), and goethite (α-FeOOH), which are not possible to distinguish from magnetite solely on the basis of their chemical composition. Nevertheless, natural hematite and goethite are usually present in much finer grain sizes than the identified magnetite. The magnetic results from sections 3.1 and 3.2 validate this assumption, since the concentration parameter describes mainly the soft (magnetite-like) fraction, which shows an increase and coarsening trend from upstream to downstream sites.

[34] Particle class 2 contains all iron oxide phases with a significant amount (>0.5 wt %) of Ti (Figure 6b), such as titanomagnetite, pseudobrookite
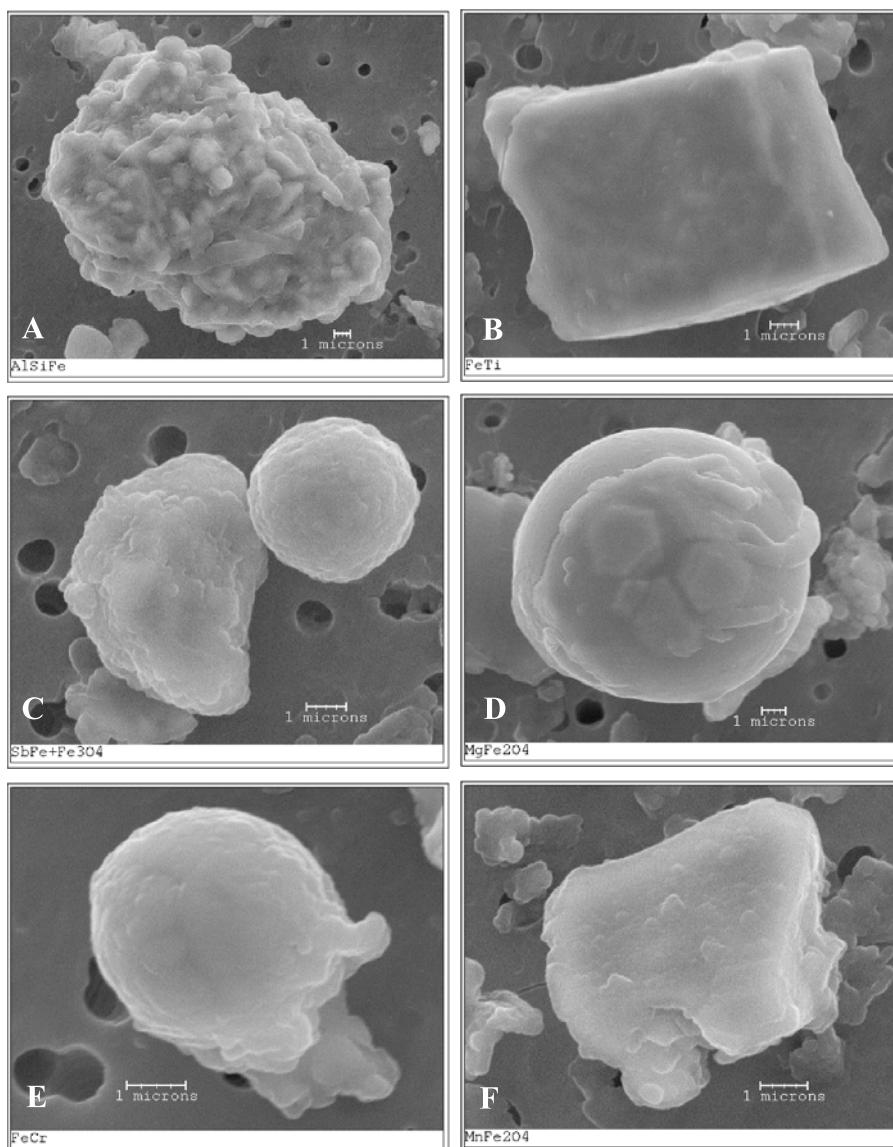
Figure 6. SEM micrographs of some exemplary particles originating from the six identified particles classes (for details see section 4). (a) Agglomerate of small pure iron oxides mixed with clay minerals, originating from natural soil weathering; (b) detrital Ti-rich iron oxide particle (titanomagnetite) from bed rock weathering; (c) anthropogenic Sb-rich particle (on the left) and anthropogenic iron oxide spherule (on the right); (d) anthropogenic iron oxide spherule with Mg-rich inclusions of magnesioferrite; (e) Cr-rich iron oxide spherule; and (f) irregular Mn-rich scoria particle.

as well as members of the ilmenite-hematite solid solution series. In general, these particles are slightly coarser than the particles from class 1. These Fe-Ti oxides usually have an irregular shape, typical of natural detrital particles derived from, for example, weathering of igneous rocks. Ti-rich particles are well known to be very resistant to any kind of dissolution and have therefore a high preservation potential [e.g., *Dillon and Franke*, 2009]. It is very likely that within some of these natural Fe-Ti oxide particles, a close paragenesis of titanomagnetite and ilmenohematite may occur [e.g., *McEnroe et al.*, 2001].

[35] Pure iron oxides that contain a detectable amount of Sb (>0.5 wt %) are sorted in particle class 3. Sb-containing particles can clearly be attributed to an anthropogenic origin [e.g., *Grousset et al.*, 1995; *Shotyk et al.*, 2005]. The measured Sb constitutes between 0.5 and 10 wt % of the elemental composition and is incorporated into pure iron oxides, which are most likely magnetite particles (Figure 6c, grain on the left). The Sb-containing particles are probably even more abundant than the observed 1 to 10% in total particle proportion, since the EDS detection limit is restricted to 0.5 wt %.

[36] Mg-rich iron oxides (e.g., magnesioferrite, see Figure 6d) form particle class 4. In some grains a minor contribution of Mn was additionally detected. The Mg-rich oxides were found in multiple shapes, as spherules or in irregular shape, but rather typical for scoria particles [*Jordanova et al.*, 2004]. They are typical products of industrial combustions [*Yan et al.*, 2005] as magnesioferrite particles, both as isolated grains or incorporated within a silicate glass matrix.

[37] Particle class 5 consists of Cr-rich iron oxides, excluding nonmagnetic chromites, which are very resistant to any chemical dissolution and at least partially of industrial origin (Figure 6e). The Mn-rich iron oxides of particle class 6, appearing as Mn glasses, are much more susceptible to chemical alteration/dissolution compared to the Cr-rich particles or pure Si glasses (Figure 6f).

[38] Pure iron oxides (class 1) are the major magnetic components (ranging between 31 and 79%) in all samples analyzed with the SEM ACC technique (see Figure 7a and Table 4). The second most abundant mineral phases are the Ti-rich iron oxides (class 2) representing about 5–52% of the magnetic fraction (see Figure 7b and Table 4). We observe a clear decreasing trend in the proportion of Ti-rich iron oxides downstream of all river segments, which is compensated by an increasing downstream proportion of pure iron oxides. The abundance of class 3 particle (Sb-rich iron oxides of anthropogenic origin (Figure 7c and Table 4)) also increases downstream suggesting that class 1 and 3 may share the anthropogenic origin. The third most abundant particle type are the Mg-rich iron oxides (class 4), with a proportion ranging from 3 to 14% (Figure 7d and Table 4). Since their origin is most likely from industrial sources, it is not surprising that their downstream proportion is also increasing. Cr-rich (1 to 5%) and Mn-rich iron oxides (2 to 13%) do not show any particular downstream trends (Figures 7e and 7f), with exception for upstream Marne and Grand Morin sites, which show the highest observed values (Table 4). For all samples a relatively high amount of pyrite particles was detected in the density separates, which amounts to approximately 40% of the total heavy mineral fraction.

5. Environmental Fingerprints in the Seine Watershed

[39] The different environmental magnetic and electron microscopic techniques discussed in sections 3

and 4 yield consistent results. We will now briefly summarize the main results and discuss them in order to interpret the different particle proportions identified in the suspended material and to examine the implications of this environmental fingerprinting method for the Seine river watershed.

[40] We observed a watershed-wide downstream increase in magnetic concentration which plateaus upon reaching Paris (Figure 8a). This correlates very well with the SEM observations of a downstream proportional increase of class 1 particles (Figure 8b). We assume that the Ti-rich iron oxides originate from mechanical weathering of the landscape and are representative of natural detrital input. Therefore, the fraction of detrital input in the total suspended particle load decreases downstream throughout the watershed (Figure 7b). Our magnetic concentration proxy M_s increases downstream similarly to the abundance of pure iron oxide particles (class 1; compare Figure 7a with Figure 8a). One can therefore deduce that the dominant control on total magnetic concentration is not the detrital fraction of the suspended particle load. Figure 8c also depicts this change in magnetomineralogy for all investigated profiles starting from rather hard coercivities upstream to much softer magnetomineralogy downstream. This agrees with the observed decreasing downstream abundance of Ti-rich iron oxides, given that the coercivity of titanomagnetite and ilmenohematite are in general higher than that of pure magnetite [e.g., *Dillon and Franke*, 2009, and references therein]. Moreover, low-temperature magnetic measurements also showed an increasing dominance of magnetite-like behavior and disappearance of goethite and hematite-like behaviors downstream through the watershed.

[41] Among the two smallest drainage areas investigated, the magnetic assemblage of the Grand Morin is characterized by relatively high coercivity and fine mean particle size in contrast to the larger rivers (Aube, Marne, and Seine), where trends of coarsening grain sizes coupled with increasing concentrations and decreasing coercivity are observed. These trends, attributed to industrialized plants and urban areas dilute quite rapidly the rural signal from the small Grand Morin drainage area.

[42] In contrast, the Orge river which has a smaller drainage area, comparable to that of the Grand Morin, seems to have a much more important impact, thus a more important contribution in pollution, on the total particle input in the Seine. The similar magnetic behavior of site 12 in the
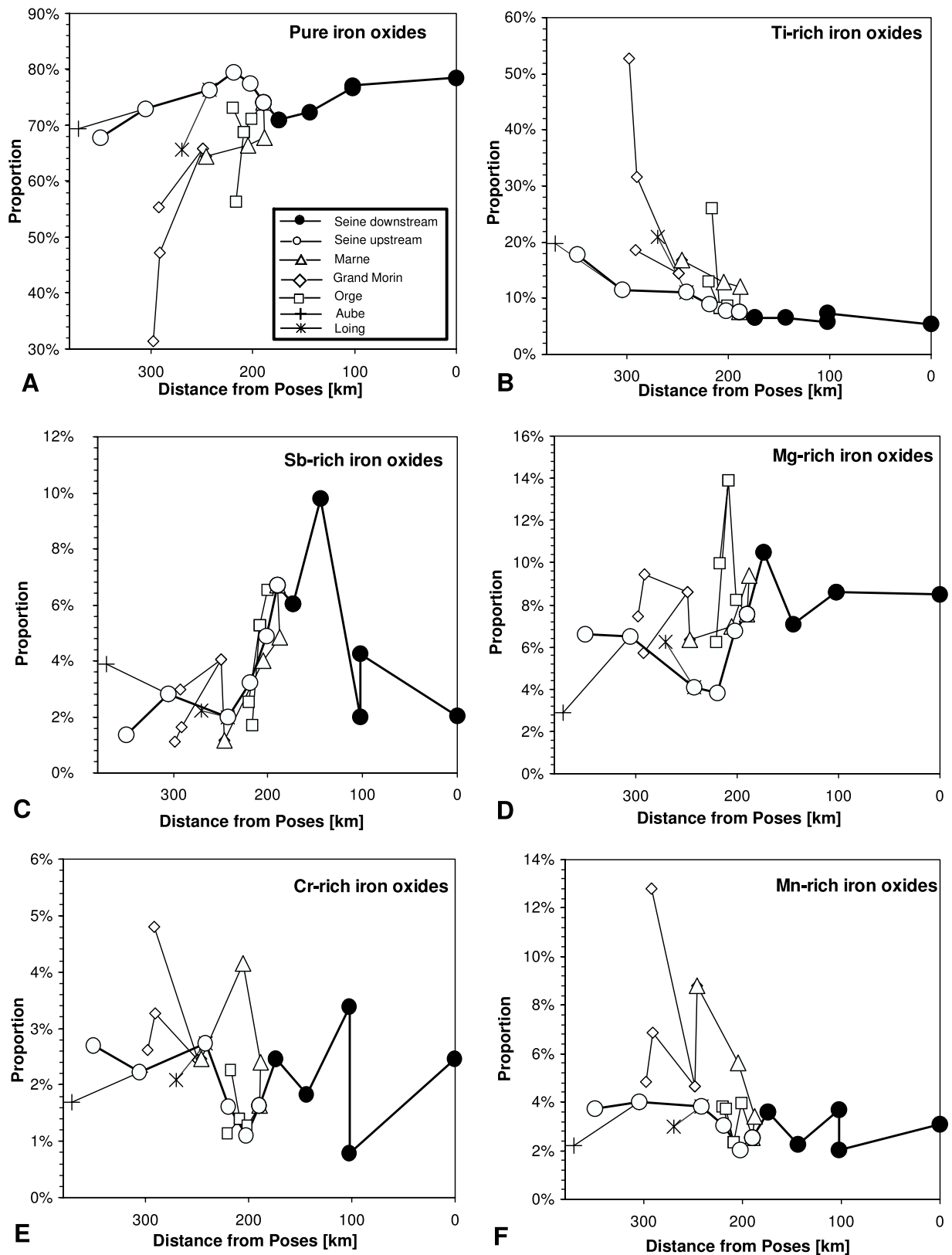
Figure 7. Schematic river-wise presentation of the proportions derived from SEM ACC analysis with respect to the distance from the last sample site Poses: (a) pure iron oxides, particles class 1; (b) Ti-rich iron oxides, particle class 2; (c) Sb-rich iron oxides, particle class 3; (d) Mg-rich iron oxides, particle class 4; (e) Cr-rich iron oxides, particle class 5; and (f) Mg-rich iron oxides, particle class 6.
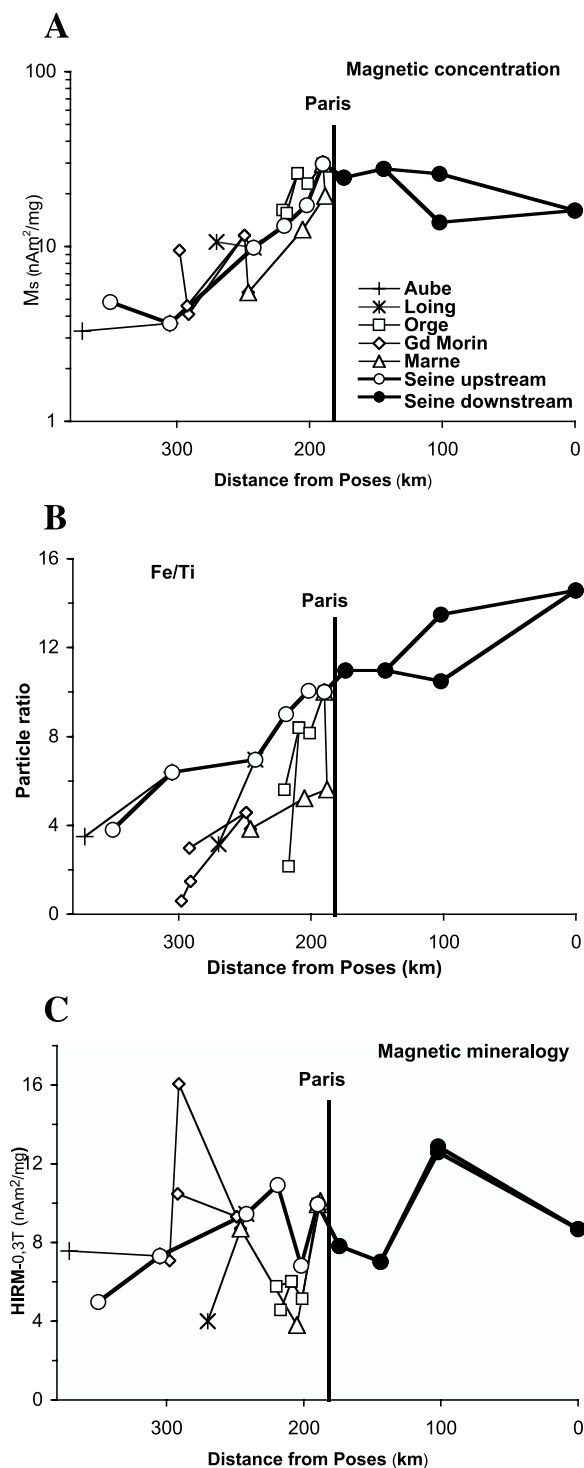
Figure 8. Schematic river-wise presentation with respect to the distance from the last sample site Poses of (a) the magnetic concentration parameter M_s, (b) the particle ratio of pure iron oxides to Ti-rich iron oxides, and (c) the magnetomineralogy parameter HIRM$_{-0.3T}$.

Seine and those within the Orge (presented in section 3.1) provides convincing evidence. The major sources for magnetic particles in the Orge

are most likely the anthropogenic pollution from the Orly city airport and the area's dense urbanization. The general change from a fine-grained, high-coercivity dominated magnetic assemblage upstream or in rural sites (e.g., Egly) to a coarser-grained magnetite-dominated particle assemblage in downstream sites results from the progressive input of anthropogenic pollution.

[43] The analysis of the various smaller and larger tributary streams therefore provides a reasonable estimation of the individual contributions to the collective particle load at any point of the river course. Each river segment has a distinct magnetic signal that allows the identification of local point sources, such as the wastewater plant at Andrésy. In future research our approach could be used to quantify pollution budgets of identified point sources and tributary river contributions.

[44] Coarse-grained MD magnetite components are very typical indicators for anthropogenic pollution particles, such as fly ashes from industrial combustion processes or emission of cars and ships [e.g., *Yang et al.*, 2007, and references therein]. In contrast, fine-grained goethite is rather a typical product of soil weathering processes [*Jambor and Dutrizac*, 1998]. Microcrystalline hematite overgrowths on oxidized magnetite or other, e.g., siliceous grains were described as a conversion product of aged ferrihydrite coatings [*Walker et al.*, 1981; *Freeman*, 1986] typical of fluvial material [e.g., *Franke et al.*, 2007b]. The mean grain sizes of samples shown in Figure 3 are typical values of coarse PSD (near MD) magnetite comparable to values reported for fluvial material by *Desenfant et al.* [2004] in the Arc river in southern France. *Robertson et al.* [2003] also describe such coarse (MD) and soft magnetite particles as typical anthropogenic particles in the urban pollution of Manchester (UK). Therefore it is very likely that magnetic particle fraction identified in the downstream sites of the Seine originate from the heavily urbanized Paris area.

[45] To further demonstrate the applied character of the environmental magnetic fingerprinting, we show in Figure 9a the regional distribution of Sb-containing iron oxides (anthropogenic origin) normalized to the amount of Ti-rich iron oxides (detrital origin). The observed trend is similar to that of magnetic concentration attributed to changes in abundance of class 1 particle (pure iron oxide (Figure 8b)). Abundance of Sb-rich iron oxides and magnetic concentration are linearly related with a very high correlation coefficient of
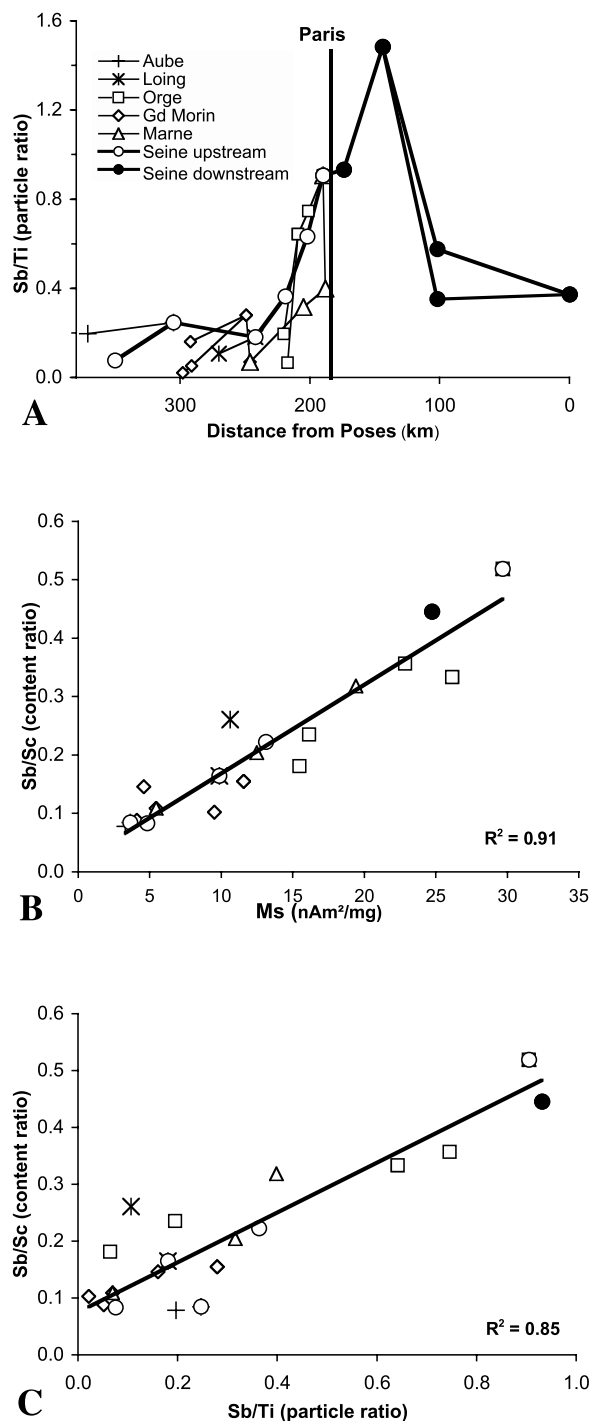
A

B

C

Figure 9. (a) Schematic river-wise presentation of the particle ratio between the Sb-rich and Ti-rich iron oxides with respect to the distance from the last sample site Poses. (b) Correlation between the Sb-rich particle ratio and the magnetic concentration parameter M_s. (c) Correlation between the Sb/Sc content ratio (data taken from *Tessier* [2003]) and the Sb/Ti particle ratio. R^2 is the Pearson's correlation coefficient.

$r^2 = 0.91$ (Figure 9b). Since the source of Sb must be anthropogenic [*Grousset et al.*, 1995; *Shotyk et al.*, 2005], this high positive correlation indicates that magnetic concentration (here saturation magnetization M_s of the 0.3 T hysteresis loops) can be used as a proxy parameter, to the first order, for anthropogenic pollution and more specifically as a tracer of Sb-rich particle concentrations in the Seine river system. Since the EDS's lower limit of detection is 0.5 wt %, we can assume the abundance of Sb containing magnetite is higher than observed, changing the slope of the linear regression line while not reducing the positive correlation coefficient. This assumption is also supported by the Sb elemental data, obtained from Instrumental Neutron Activation Analyses (INAA) performed on the respective bulk sediment samples [*Tessier and Bonté*, 2002]. Moreover, the high correlation ($r^2 = 0.85$) between the normalized Sb/Sc ratio (bulk sediments) and the Sb/Ti ratio from the magnetic fraction (Figure 9c) suggests that the major proportion of Sb is actually present within the magnetic (heavy mineral) fraction. Further detailed electron microscopic and geochemical investigations of these specific particles will certainly offer a more complete understanding of these (and other) anthropogenic particle types.

6. Conclusion

[46] In this innovative study the potential of environmental magnetism techniques, as a tool to describe multivariate particle flux in a complex river system, is shown in the Seine drainage area of northern France. We showed that combining environmental magnetic measurements and qualitative SEM analyses is a straightforward method, facilitating particle discrimination in river systems and in particular the detection of anthropogenic pollution, such as for example Sb and other heavy metals. The approach calculates the absolute particle flux ratios and traces point sources for distinct particle input. The method also enables the separation of different particle classes, such as pure iron oxides, Ti-rich, Mg-rich, Sb-containing, Mn-rich or Cr-rich iron oxides.

[47] Clear trends were observed in the Seine river system, such as a general increase in magnetic concentration from upstream to downstream regions coupled with a downstream "softening" trend in the magnetic assemblage. These tendencies could be successfully linked to an increasing input of anthropogenic magnetite supported by the results from the SEM ACC analyses. Additionally, detailed conclusions can be drawn with respect to

local anomalies, because these are easily detectable as "outliers" from the general trend line of the respective river segment. Therefore point sources of specific particulate matter could be identified, such as the effluence of the wastewater plant at Andrésy northwest of Paris, from hematite specific magnetic behavior.

[48] Our approach provides straightforward means of characterizing and quantifying the (magnetic) particle flux in the Seine river system, and can be easily adapted to investigate other (major) river systems in the World.

Acknowledgments

References

Chaparro, M. A. E., J. C. Bidegain, A. M. Sinito, S. S. Jurado, and C. S. G. Gogorza (2004), Magnetic studies applied to different environments (soils and stream sediments) from a relatively polluted area in Buenos Aires Province, Argentina, *Environ. Geol.*, *45*, 654–664, doi:10.1007/s00254-003-0915-x.

Day, R., M. Fuller, and V. Schmidt (1977), Hysteresis properties of titanomagnetites: Grain-size and compositional dependence, *Phys. Earth Planet. Inter.*, *13*, 260–267, doi:10.1016/0031-9201(77)90108-X.

Dekkers, M. J. (1989), Magnetic properties of natural goethite II. TRM behaviour during thermal and alternating field demagnetization and low-temperature treatment, *Geophys. J.*, *97*, 341–355, doi:10.1111/j.1365-246X.1989.tb00505.x.

Desenfant, F., E. Petrovsky, and P. Rochette (2004), Magnetic signature of industrial pollution of stream sediments and correlation with heavy metals: Case study from south France, *Water Air Soil Pollut.*, *152*, 297–312, doi:10.1023/B:WATE.0000015356.88243.f0.

Dillon, M., and C. Franke (2009), Diagenetic alteration of natural magnetic Fe-Ti oxides identified by energy dispersive spectroscopy (EDS) and low temperature remanence and hysteresis measurements, *Phys. Earth Planet. Inter.*, *172*, 141–156, doi:10.1016/j.pepi.2008.08.003.

Dunlop, D. J. (2002), Theory and application of the Day plot (M_{rs}/M_s versus H_{cr}/H_c): 1. Theoretical curves and tests using titanomagnetite data, *J. Geophys. Res.*, *107*(B3), 2056, doi:10.1029/2001JB000486.

Dunlop, D. J., and Ö. Özdemir (1997), *Rock Magnetism: Fundamentals and Frontiers*, 573 pp., Cambridge Univ. Press, Cambridge, U. K.

Evans, M. E., and F. Heller (2003), *Environmental Magnetism: Principles and Applications of Enviromagnetics*, Academic, Paris.

Franke, C., T. Frederichs, and M. J. Dekkers (2007a), Efficiency of heavy liquid separation to concentrate magnetic particles, *Geophys. J. Int.*, *170*(3), 1053–1066, doi:10.1111/j.1365-246X.2007.03489.x.

Franke, C., T. von Dobeneck, M. R. Drury, J. D. Meeldijk, and M. J. Dekkers (2007b), Magnetic petrology of equatorial Atlantic sediments: Electron microscopic results and their environmental magnetic implications, *Paleoceanography*, *22*, PA4207, doi:10.1029/2007PA001442.

Frederichs, T., T. von Dobeneck, U. Bleil, and M. J. Dekkers (2003), Towards the identification of siderite, rhodochrosite and viviantite in sediments and their low-temperature magnetic properties, *Phys. Chem. Earth,*, *28*, 669–679.

Freeman, R. (1986), Magnetic mineralogy of pelagic limestones, *Geophys. J. R. Astron. Soc.*, *85*, 433–452.

Garming, J. F. L., U. Bleil, C. Franke, and T. von Dobeneck (2007), Low-temperature partial magnetic self-reversal in marine sediments by magnetostatic interaction of titanomagnetite and titanohematite intergrowths, *Geophys. J. Int.*, *170*(3), 1067–1075, doi: 10.1111/j.1365-246X.2007.03504.x.

Georgeaud, V. M., P. Rochette, J. P. Ambrosi, D. Vandamme, and D. Williamson (1997), Relationship between heavy metals and magnetic properties in a large polluted catchment: The Etang de Berre (south of France), *Phys. Chem. Earth*, *22*(1–2), 211–214, doi:10.1016/S0079-1946(97)00105-5.

Grousset, F. E., C. R. Quetel, B. Thomas, O. F. X. Donard, C. E. Lambert, F. Guillard, and A. Monaco (1995), Anthropogenic vs. lithogenic origins of trace elements (As, Cd, Pb, Rb, Sb, Sc, Sn, Zn) in water column particles: Northwestern Mediterranean Sea, *Mar. Chem.*, *48*(3–4), 291–310, doi:10.1016/0304-4203(94)00056-J.

Hatfield, R. G., and B. A. Maher (2008), Suspended sediment characterization and tracing using a magnetic fingerprinting technique: Bassenthwaite Lake, Cumbria, UK, *Holocene*, *18*(1), 105–115, doi:10.1177/0959683607085600.

Horowitz, A. J., M. Meybeck, Z. Idlafkih, and E. Biger (1999), Variations in trace element geochemistry in the Seine river basin based on floodplain deposits and bed sediments, *Hydrol. Processes*, *13*(9), 1329–1340, doi:10.1002/(SICI)1099-1085(19990630)13:9<1329::AID-HYP811>3.0.CO;2-H.

Jambor, J. L., and J. L. Dutrizac (1998), Occurrence and constitution of natural and synthetic ferrihydrite: A widespread iron oxyhydroxide, *Chem. Rev.*, *98*, 2549–2585, doi:10.1021/cr970105t.

Jordanova, D., V. Hoffmann, and K. T. Fehr (2004), Mineral magnetic characterization of anthropogenic magnetic phases in the Danube river sediments (Bulgarian part), *Earth Planet Sci. Lett.*, *221*, 71–89, doi:10.1016/S0012-821X(04)00074-3.

Kakol, Z., J. Sabol, J. Stickler, A. Kozlowski, and J. M. Honig (1994), Influence of titanium doping on the magnetocrystalline anisotropy of magnetite, *Phys. Rev. B*, *49*, 12,767–12,772.

Kosterov, A. (2003), Low-temperature magnetization and AC susceptibility of magnetite: Effect of thermomagnetic history, *Geophys. J. Int.*, *154*, 58–71, doi:10.1046/j.1365-246X.2003.01938.x.

Lagroix, F., S. K. Banerjee, and M. J. Jackson (2004), Magnetic properties of the Old Crow tephra: Identification of a complex iron titanium oxide mineralogy, *J. Geophys. Res.*, *109*, B01104, doi:10.1029/2003JB002678.

Lowrie, W., and F. Heller (1982), Magnetic properties of marine limestones, *Rev. Geophys.*, *20*, 171–192, doi:10.1029/RG020i002p00171.

Maher, B. A., and R. Thompson (1999), *Quaternary Climates: Environments and Magnetism*, 390 pp., Cambridge Univ. Press, Cambridge, U. K.

McEnroe, S. A., P. Robinson, and P. T. Panish (2001), Aeromagnetic anomalies, magnetic petrology, and rock magnetism of hemoilmenite- and magnetite-rich cumulate rocks from the Sokndal Region, South Rogaland, Norway, *Am. Mineral.*, *86*, 1447–1468.

Meybeck, M., G. De Marsily, and E. Fustec (1998), *La Seine en son bassin: Fonctionnement écologique d'un système fluvial anthropisé*, 752 pp., Elsevier, Paris.

Morin, F. J. (1950), Magnetic susceptibility of alpha Fe_2O_3 and alpha Fe_2O_3 with added Titanium, *Phys. Rev.*, *78*(6), 819–820, doi:10.1103/PhysRev.78.819.2.

Morrish, A. H. (1995), *Canted Antiferromagnetism: Hematite*, 208 pp., World Sci., Singapore.

Özdemir, Ö., and D. J. Dunlop (2003), Low-temperature behaviour and memory of iron-rich titanomagnetites (Mt. Haruna, Japan and Mt. Pinatubo, Philippines), *Earth Planet. Sci. Lett.*, *216*, 193–200, doi:10.1016/S0012-821X(03)00481-3.

Özdemir, Ö., D. J. Dunlop, and B. M. Moskowitz (1993), The effect of oxidation on the Verwey transition in magnetite, *Geophys. Res. Lett.*, *20*, 1671–1674, doi:10.1029/93GL01483.

Özdemir, Ö., D. J. Dunlop, and B. M. Moskowitz (2002), Changes in remanence, coercivity and domain state at low temperature in magnetite, *Earth Planet. Sci. Lett.*, *194*, 343–358, doi:10.1016/S0012-821X(01)00562-3.

Robertson, D. J., K. G. Taylor, and S. R. Hoon (2003), Geochemical and mineral magnetic characterization of urban sediment particulates, Manchester, UK, *Appl. Geochem.*, *18*, 269–282, doi:10.1016/S0883-2927(02)00125-7.

Robin, E., and E. Molino (2006), Chronostratigraphy, composition, and origin of Ni-rich spinel from the Late Eocene Fuente Caldera section in Spain: One impact or more?, *Meteorit. Planet. Sci.*, *41*(8), 1231–1248.

Robin, E., D. Boclet, P. Bonté, L. Froget, C. Jéhanno, and R. Rocchia (1991), The stratigraphic distribution of Ni-rich spinels in Cretaceous-tertiary boundary rocks at El Kef (Tunesia), Caravaca (Spain) and Hole 761C (Leg122), *Earth Planet. Sci. Lett.*, *107*, 715–721, doi:10.1016/0012-821X(91)90113-V.

Robin, E., C. Rabouille, G. Martinez, I. Lefevre, L. Reyss, P. van Beek, and C. Jeandel (2003), Direct barite determination using SEM/EDS-ACC system: Implication for constraining barium carriers ad barite preservation in marine sediments, *Mar. Chem.*, *82*, 289–306, doi:10.1016/S0304-4203(03)00075-6.

Roy, S., J. Gaillardet, and C. J. Allègre (1999), Geochemistry of dissolved and suspended loads of the Seine river, France: Anthropogenic impact, carbonate and silicate weathering, *Geochim. Cosmochim. Acta*, *63*(9), 1277–1292, doi:10.1016/S0016-7037(99)00099-X.

Shotyk, W., M. Krachler, and B. Chen (2005), Anthropogenic impacts on the biogeochemistry and cycling of antimony, *Metal Ions Biol. Syst.*, *44*, 171–203.

Stoner, J. S., J. E. T. Channell, and C. Hillaire-Marcel (1996), The magnetic signature of rapidly deposited detrital layers from the deep Labrador Sea: Relationship to North Atlantic Heinrich layers, *Paleoceanography*, *11*, 309–325, doi:10.1029/96PA00583.

Tessier, L. (2003), Transport et caractérisation des matières en suspension dans le bassin versant de la Seine: Identification de signatures naturelles et anthropiques, Ph.D. thesis, 344 pp., Ecole Natl. des Ponts et Chaussées, Paris.

Tessier, L., and P. Bontè (2002), Suspended sediment transfer in Seine river watershed, France: A strategy using fingerprinting from trace elements, in *Proceedings of Science for Water Policy (SWAP): The Implications of the Water Framework Directive*, edited by L. Ledoux and D. Burgess, pp. 79–99, Univ. of East Anglia, Norwich, U. K.

Thompson, R., and F. Oldfield (1986), *Environmental Magnetism*, 227 pp., Allen and Unwin, London.

Turner, R. E., and N. N. Rabalais (1991), Changes in Mississippi river water quality this century and implication for coastal food webs, *BioScience*, *41*(3), 140–147, doi:10.2307/1311453.

Verwey, E. J. M. (1935), The crystal structure of γ-F_2O_3 and γ-Al_2O_3, *Z. Kristallogr.*, *91*, 65–69.

Walker, T. R., E. E. Larson, and R. P. Hoblitt (1981), Nature and origin of hematite in the Moenkopi formation (Triassic), Colorado plateau: A contribution to the origin of magnetism in red beds, *J. Geophys. Res.*, *86*, 317–333, doi:10.1029/JB086iB01p00317.

Yan, S., S. Sun, and S. Jahanshahi (2005), Reactions of dense MgO with calcium ferrite-based slags at 1573 K, *Metall. Mater. Trans. B*, *36*, 651–656.

Yang, T., L. Qingsheng, C. Lungsang, and L. Zhendong (2007), Magnetic signature of heavy metal pollution of sediments: Case study from the East Lake in Wuhan, China, *Environ. Geol.*, *52*, 1639–1650, doi:10.1007/s00254-006-0609-2.